IEEE Access
Multidisciplinary | Rapid Review | Open Access Journal

IEEE POWER & ENERGY SOCIETY SECTION

Received 18 November 2023, accepted 5 December 2023, date of publication 7 December 2023,
date of current version 13 December 2023.

*Digital Object Identifier 10.1109/ACCESS.2023.3340855*

RESEARCH ARTICLE

# E-Core and C-Core Switched Flux Permanent Magnet Generators for Wind Power Generation

**PATTASAD SEANGWONG[1], NUWANTHA FERNANDO[2], (Member, IEEE), APIRAT SIRITARATIWAT[1], AND PIRAT KHUNKITTI[1], (Member, IEEE)**

[1]Department of Electrical Engineering, Faculty of Engineering, Khon Kaen University, Khon Kaen 40002, Thailand
[2]School of Engineering, Royal Melbourne Institute of Technology (RMIT), Melbourne, VIC 3000, Australia

Corresponding author: Pirat Khunkitti (piratkh@kku.ac.th)

This work was supported in part by the National Research Council of Thailand and Khon Kaen University under Grant N42A660360, and in part by the National Research Council of Thailand under Grant N41A660159.

**ABSTRACT** This paper introduces a 6-phase switched flux permanent magnet (SFPM) generator with high permanent magnet (PM) utilization, designed for a 2 kW wind power generation application. Two different SFPM generator variants were designed and analyzed by applying E-core and C-core techniques to a state-of-the-art (SOTA) benchmark SFPM machine structure. Key design variables, namely, the rotor pole number, split ratio, rotor pole width, and the number of turns per coil were optimized. The electromagnetic performance, specifically as a wind generator considering objectives of achieving high PM utilization, minimizing voltage waveform distortion, and reducing cogging torque, was evaluated using finite element analysis. The results obtained from the analysis demonstrated that both the E-core and C-core SFPM generators exhibited significantly higher flux-linkage per unit PM volume compared to the SOTA benchmark generator. In particular, the optimized C-core SFPM generator demonstrated nearly double the magnet utilization, half the cogging torque, and higher efficiency when compared to the benchmark SFPM generator. Notably, the C-core SFPM generator achieved a power per PM volume of 24,979 kW/m$^3$, positioning it as the second-highest performing PM generator among all SOTA generators. Lastly, a prototype of the 6-phase 12-stator/25-rotor C-core SFPM generator was manufactured and tested to validate the analytical design.

**INDEX TERMS** Permanent magnet generators, switched flux permanent magnet machine, E-core, C-core, wind power generation.

## I. INTRODUCTION

Wind power generation has attracted great attention in the last decade since renewable energy generation is becoming an unavoidable trend, consequently extensive research and development efforts have been dedicated to advancing wind turbine generators. Permanent magnet (PM) machines are the leading choice as wind power generators due to their numerous advantages, including the absence of excitation losses, high torque and power output, and enhanced reliability [1], [2], [3]. PM machines can be designed as rotor PM machines, which have PMs mounted on the rotor, and stator PM machines, which have PMs attached to the stator [4], [5], [6]. Stator PM machines are particularly appealing for low-speed wind power generation, as they typically exhibit lower inertia and higher robustness compared to rotor PM machines [5], [6]. Within the category of stator PM machines, three different configurations are commonly utilized: doubly salient permanent magnet machines, flux reversal permanent magnet machines, and switched flux permanent magnet (SFPM) machines [5], [6], [7], [8]. Of these configurations, SFPM machines have attracted significant research attention due to their potential improvements in power and torque capability, highly symmetric sinusoidal back-electromotive force (EMF), high reliability, low risk of demagnetization, and a simple structure with high robustness [9], [10], [11], [12]. The stator of a SFPM machines can also be manufactured in modular, which holds the potential to reduce installation costs in wind power applications.

Past developments of stator-SFPM machines have primarily focused on enhancing torque density, reducing ripple and cogging torque, and achieving symmetrical properties of the

The associate editor coordinating the review of this manuscript and approving it for publication was Sinisa Djurovic.

back-EMF, as evidenced by the following selected literature. In 2010, an E-core switched flux brushless machine was introduced, which utilized only half the magnets compared to conventional structures [13]. This innovation resulted in an improved back-EMF and electromagnetic torque. Building upon this, Chen et al. presented a SFPM machine with the C-core design [14]. This design not only increased the utilization of permanent magnets and torque capability but also provided a larger slot area for the stator winding. Several SFPM machines with multiphase configurations were designed to meet the demanding requirements of high-reliability applications [15], [16], [17], [18], [19], [20]. a six-phase hybrid-excited SFPM machine utilizing both E-core and C-core stators demonstrated enhanced fault-tolerance through improved physical and magnetic isolation between phase windings [21]. In 2021, a novel H-type modular stator core with flux-focusing was introduced, which exhibited remarkable high torque capability [22]. Continuing research efforts have resulted in further advancements in the field [23], [24], [25], [26], [27], [28], leading SFPM machines to be regarded as promising solutions for high-torque and wide-speed-range applications.

Based on extensive literature surveys, it is evident that the majority of research on SFPM machines has primarily focused on motor operation. However, several noteworthy studies have indicated that stator-SFPM machines are highly capable of wind power generation. In 2015, a 9-phase 36-stator/34-rotor pole SFPM machine was specifically designed for low-speed and high-torque wind power generation [29]. F. Li et al. conducted extensive design and optimization work on this machine, further highlighting its capabilities [30]. The potential of SFPM generators for geared wind generator has been extensively considered [31], [32], demonstrating its high torque capability and suitability for medium-speed wind power generation. L. Shao et al. proposed a 12-phase redundant SFPM generator for wind power generation [33]. This generator achieves high power density and can be considered as the state-of-the-art (SOTA). Later on, a comparative study conducted between a 12-phase SFPM generator proposed in [33] and a 9-phase SFPM generator proposed in [29] exclusively for wind power generation provides compelling evidence supporting the superior performance of multi-phase SFPM machines in this application [34]. Additionally, the electromagnetic performance of 12-phase SFPM machines was demonstrated to outperform surface-PM machines [35]. The suitability of a SFPM generator for wind applications was still affirmed in recent research [36], emphasizing their continued relevance and potential in the field.

Past research undeniably demonstrates that the SFPM machine holds great promise as a wind power generator. However, the majority of existing SFPM generators face challenges related to high PM usage, resulting in concerns regarding low PM utilization and high manufacturing costs, as the cost of PMs is typically 30% or more of total machine cost. High stator complexity and a narrow armature slot area are also weaknesses of such SFPM generators. Addressing these drawbacks necessitates further research and development in the field. This paper proposes SFPM generator structures and optimization for requirements specifically considering application as wind power generators, namely, improving the PM utilization, minimizing voltage waveform distortion by evaluation of total harmonic distortion (THD), lower vibration by minimizing the cogging torque and evaluation of voltage regulation. In this context, the novelties of this work are the following: 1) the first to report the application of E-core and C-core design techniques for PM generator purposes and 2) analysis of the PM utilization of three different SFPM machines. Regarding to the findings, a SFPM generator with an extremely high PM utilization has been discovered in this study. Finally, the prototyping of the most suitable structure was conducted to validate the design simulations and analysis.

The next section presents the SFPM machine configuration in detail with definitions of the physical dimensions of the different variants. Section III presents the optimization study of the E-core and C-core designs. Section IV presents the evaluation of performance using finite element analysis (FEA) and Section V presents the prototype SFPM machine, experimental validation. Section VI provides a conclusion with the key findings of this research.

## II. MACHINE CONFIGURATION

The SFPM machine served as a baseline in our research for benchmarking purposes is a scaled-down version of the optimized SOTA 24/22 (stator-/rotor-pole) SFPM generator [33], as depicted in Fig. 1(a). This machine can be configured to incorporate a maximum of 12 phases. Detailed dimensions of this benchmark machine can be found in Table 1. It is important to highlight that the SOTA benchmark machine has already undergone optimization and achieves remarkable power density when compared to other existing SFPM generators. The structure of the SOTA benchmark SFPM generator contains PMs arranged between two stator pieces, in which the PMs are magnetized circumferentially in the opposite direction. The concentrated armature winding is inserted into the openings of the stator slots.

In this research, two variants of the SFPM machine are introduced, namely, the E-core and C-core generators. The topology of the proposed E-core and C-core generators following optimization of structural design variables is shown in Figs. 1(b) and 1(c) respectively and their dimensions are given in Table 1. The E-core structure comprises 12 E-shaped segments, which are arranged circumferentially and sandwiched between the PMs with alternating polarity. The C-core structure, as shown in Fig. 1(c), builds upon the E-core design by eliminating the mid-partitioning stator teeth. This modification increases the slot area available for armature winding installation, further improving the generator's capabilities. Both the E-core and C-core structures incorporate approximately half the amount of PMs compared to the SOTA benchmark SFPM structure. It is important to note that while the individual coils of the SOTA benchmark SFPM machine

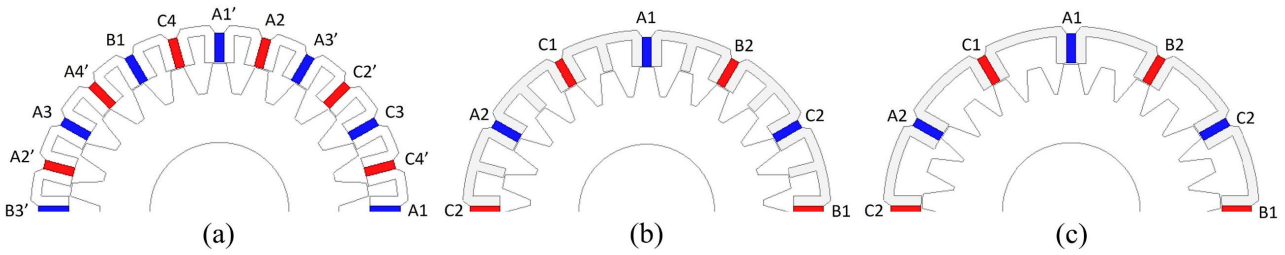


**FIGURE 1.** Cross-section of: (a) SOTA benchmark 12-phase 24-stator/22-rotor generator [33], (b) optimal 6-phase 12-stator/23-rotor E-core generator and (c) optimal 6-phase 12-stator/25-rotor C-core generator.

**TABLE 1.** Dimension of SFPM generators.

| Parameters | Unit | SOTA benchmark | E-core | C-core |
|---|---|---|---|---|
| Number of phases | phase | 12 | 6 | |
| Number of stator pole, $N_s$ | pole | 24 | 12 | |
| Number of rotor pole, $N_r$ | pole | 22 | 23 | 22 |
| PM type | - | | Nd-Fe-B | |
| Magnet remanence | T | | 1.2 | |
| Magnet coercivity | kA/m | | -909.46 | |
| Rated rotor speed | rpm | | 500 | |
| Stack length, $L_{st}$ | mm | | 120.25 | |
| Stator outer radius, $R_{so}$ | mm | | 106.275 | |
| Stator yoke length, $L_{sy}$ | mm | | 5.564 | |
| Split ratio | - | | 0.8 | |
| Stator inner radius, $R_{si}$ | mm | | 85.02 | |
| Cut delta length, $L_{delta}$ | mm | | 5.2 | |
| Stator pole arc, $\theta_{st}$ | ° | | 3.9375 | |
| Air gap length, g | mm | | 0.65 | |
| PM arc, $\theta_{PM}$ | ° | | 3.375 | |
| Rotor pole height, $L_{rh}$ | mm | | 16.874 | |
| Rotor inner radius, $R_{ri}$ | mm | | 39 | |
| PM length, $L_{PM}$ | mm | | 17 | |
| Stator slot arc, $\theta_{ss}$ | ° | 3.75 | 7.5 | 18.75 |
| Rotor pole width ratio | - | 1.4 | 1.5 | 1.5 |
| Rotor pole arc, $\theta_{rt}$ | ° | 5.25 | 5.625 | 5.625 |
| Rotor pole-yoke arc, $\theta_{ry}$ | ° | 12.075 | 12.938 | 12.938 |
| Coil turns, $N_{coil}$ | turn | 65 | 120 | 105 |
| Conductor cross-section | $mm^2$ | | 0.82 | |
| Normal tooth arc, $\theta_{nt}$ | ° | - | 3.75 | - |
| Total stator slot area | $mm^2$ | 2870.6 | 4965.3 | 6013.1 |
| Total magnet volume | $mm^3$ | 245.5 | 122.7 | |
| Machine volume | $cm^3$ | | 4,266.75 | |

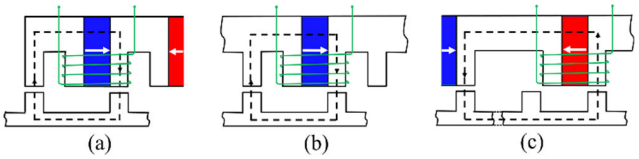


**FIGURE 2.** Flux circulation path of (a) SOTA benchmark (b) E-core and (C) C-core SFPM generators.

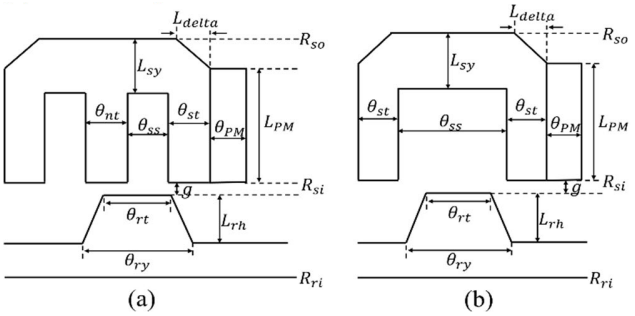


**FIGURE 3.** Design parameters of (a) E-core and (b) C-core SFPM generators.

can be configured with a maximum of 12 phases, the E-core and C-core structures are limited to a maximum of 6 phases.

Fig. 2 depicts the flux circulation of the SOTA benchmark, E-core, and C-core SFPM generators, respectively. In the case of the SOTA benchmark and C-core structures, the circulation path (dashed line) is completed by the adjacent stator teeth. On the other hand, the flux circulation in the E-core structure involves both its stator and normal teeth. The C-core structure, in particular, has a longer flux circulation path than the other structures. The design parameters utilized to optimize the structure of the E-core and C-core are illustrated in Fig. 3, and the optimization procedure is described in Section III.

## III. OPTIMIZATION OF KEY DESIGN PARAMETERS

In order to maximize the performance of both E-core and C-core SFPM generators, the impacts of the key design parameters, including the rotor pole number, split ratio, rotor pole width ratio, and the number of turns per coil, were evaluated and optimized to achieve a rated power of 2 kW at 500 rpm. The optimization process employed a stepwise approach, whereby the optimal value for each parameter was determined and retained for further optimization of the remaining design parameters. The priority given to optimizing each parameter was based on its impact on the overall design objectives. As for the wind generator, the power generating capability is a crucial index. Since the phase-EMF is closely associated with power generation capacity and quality, the maximizing the magnitude of EMF and reducing the THD were chosen as the primary optimization goal. In addition, the minimization of cogging torque plays an important role in reducing wind-turbine vibrations and turbine low speed operation. Hence, cogging torque was taken into account during the evaluation and optimization process. The optimal solution, obtained from varying each design, was chosen based on the formulation of a trade-off objective function. This function considers different weights assigned

to each design objective, outlined as follows.

$$f_{GOAL} = w_1 \frac{EMF(x_i)}{EMF'} + w_2 \frac{THD'}{THD(x_i)} + w_3 \frac{T'_{cog}}{T_{cog}(x_i)} \quad (1)$$

The optimal point is defined as the point that yields the lowest $f_{GOAL}$ value. $EMF'$, $THD'$, and $T'_{cog}$ represent the initial values of phase $EMF$, $THD$, and peak-to-peak cogging torque, respectively. $EMF(x_i)$, $THD(x_i)$, and $T_{cog}(x_i)$ correspond to their values at each key design parameter, $x_i$. The weight coefficients $w_1$, $w_2$, and $w_3$ are specifically set as 0.4, 0.2, and 0.4, respectively, to fulfill the design objective in this work.

### A. POLE NUMBER COMBINATION

The number of salient poles is a critical factor that significantly affects the performance of SFPM machines since it serves as the component that switches the magnetic flux polarity and therefore has a significant impact on magnetic field circulation behavior. Fig. 4 illustrates the impact of varying rotor pole number on the no-load EMF, THD, and peak-to-peak cogging torque of the SOTA benchmark, E-core, and C-core SFPM generators. The graph demonstrates that both E-core and C-core generators exhibit an increase in EMF as the number of rotor poles rises, reaching a maximum value at 24 rotor poles, after which it starts to decrease. In addition, the E-core and C-core generators show lower THD values with a higher number of poles due to a relatively smoother transmission of the flux switching effect. This effect typically occurs when the number of rotor poles approaches twice the number of stator poles. Analyzing the THD characteristics reveals that the number of rotor poles need to be greater than 21 to maintain an acceptable THD of less than 10%. While the no-load EMF of the E-core and C-core generators reaches its peak at 24 rotor poles, these generators exhibit high cogging torque due to the alignment of stator and rotor poles. To achieve low cogging torque and symmetrical EMF, it is essential to consider the correlation between the number of stator and rotor poles ($N_s$ and $N_r$), described as [37] and [38]:

$$\frac{N_s}{HCD\,(N_s, N_s)} = 6i \quad (2)$$

where $HCD$ is the highest common divisor and $i$ is an integer. Among the different configurations, the generators having 23 and 25 rotor poles exhibit the lowest cogging torque, along with low THD and relatively high EMF magnitude. Comparing these two options, the 23-pole E-core SFPM machine demonstrates a low THD of 2.6% and a low cogging torque of 1.4 N·m, whereas the 25-pole C-core SFPM machine achieves a low THD of 4.4% and a low cogging torque of 2.3 N·m. These configurations of E-core and C-core generators are selected for further optimization in the following subsections. It is important to note that, at this stage, the SOTA benchmark outperforms other options.

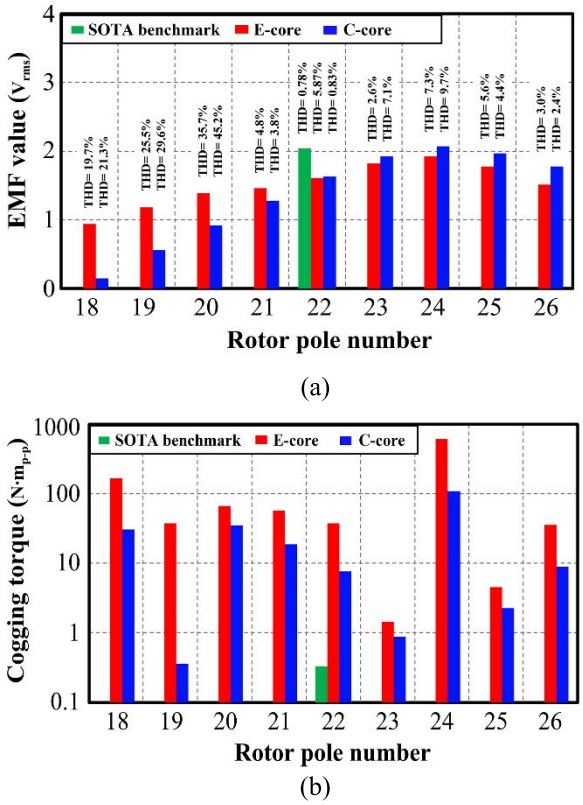


**FIGURE 4.** Influence of the number of rotor pole on the no-load characteristics of SFPM generators. (a) Phase EMF (rms value, 1 turn) and THD. (b) Cogging torque.

### B. COIL VOLTAGE VECTORS AND PHASE VOLTAGE

The voltage vectors corresponding to individual coils of the E-core and C-core SFPM generators are illustrated in Fig. 5. It is important to highlight that each phase winding of the SFPM machines requires two coils to eliminate even-order harmonics in the EMF waveform. These coils can be interconnected to form two sets of 3-phase armature windings, which further contributes to enhancing the reliability of the generator.

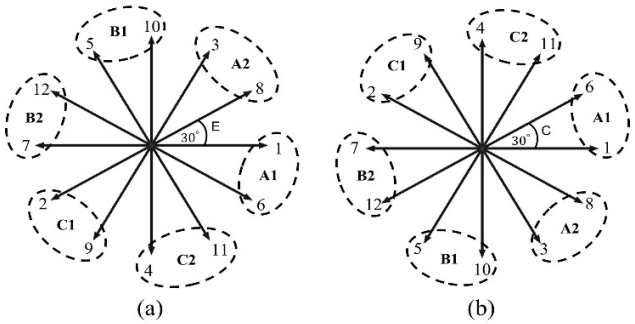


**FIGURE 5.** Phase-EMF vectors of (a) 6-phase 12-stator/23-rotor E-core and (b) 6-phase 12-stator/25-rotor C-core SFPM generators.

### C. SPLIT RATIO

The split ratio, expressed as the ratio of $R_{si}$ to $R_{so}$, plays a crucial role in influencing the magnetic flux path of a PM machine, thereby significantly impacting its electromagnetic

performance. In this section, the impact of split ratio variation on the no-load performance of the 12/23 E-core and 12/25 C-core SFPM generators is evaluated. The initial split ratio of these generators is set at 0.8, based on the value of the SOTA benchmark structure, then varied from 0.6 to 0.9. Figs. 6(a)-6(b) depict the effect of the split ratio on the phase EMF, THD, and cogging torque profiles. The results clearly show that both the E-core and C-core SFPM generators achieve the highest EMF with the lowest THD at a split ratio of 0.8. As the split ratio increases beyond this point, there is a rapid reduction in the EMF due to increased leakage flux. Although adjusting the split ratio reduces the cogging torque, the optimization process in the following section focuses on optimizing the rotor pole width ratio to minimize cogging torque, rather than adjusting the split ratio. Hence, it can be concluded that the optimal split ratio for both proposed generators is 0.8. At this optimal split ratio, both the E-core and C-core generators exhibit higher cogging torque compared to the SOTA benchmark structure. The C-core generator exhibits higher EMF, THD, and cogging torque compared to the E-core generator. The larger cogging torque of the C-core generator is attributed to the relatively higher fields at the stator teeth resulting from the modified flux paths.

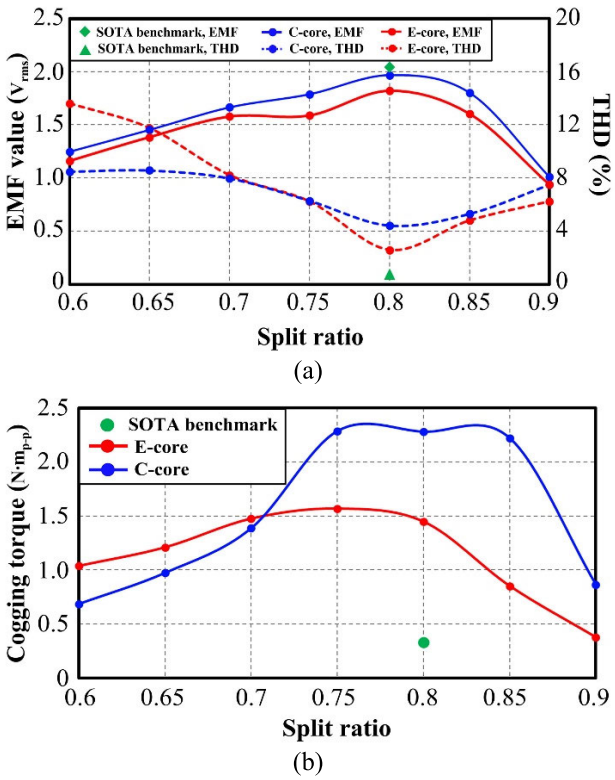


**FIGURE 6.** Influence of the split ratio on the no-load characteristics of SFPM generators. (a) Phase EMF (rms value, 1 turn) and THD. (b) Cogging torque.

rotor pole width to the stator pole pitch of 1/4 is defined as the rotor pole width ratio of 1. The impact of the rotor pole width on the no-load characteristics of the 12/23 E-core and 12/25 C-core SFPM generators with an optimal split ratio of 0.8 is analyzed, as shown in, as shown in Fig. 7(a). It can be observed that the phase EMF of both generators increases with an increasing rotor pole width ratio until it reaches its maximum value, thereafter the EMF decreases continuously due to a larger leakage flux between adjacent teeth. Furthermore, the THD of the proposed generators is small at the corresponding rotor pole width ratios that produce the highest EMF. This suggests that the magnetic flux circulation around those specific rotor pole width ratios achieves better magnet utilization. In addition, Fig. 7(b) illustrates that changes in the rotor pole width have a significant impact on the cogging torque, primarily due to its effect on restricting the air-gap magnetic field resulting from stator slotting. Based on the results, the optimal rotor pole width ratio for the E-core and C-core generators is selected as 1.5, considering its the highest EMF, acceptable THD, and minimal cogging torque. Notably, the peak-to-peak cogging of the optimal rotor pole width C-core generator is significantly lower compared to the SOTA benchmark.

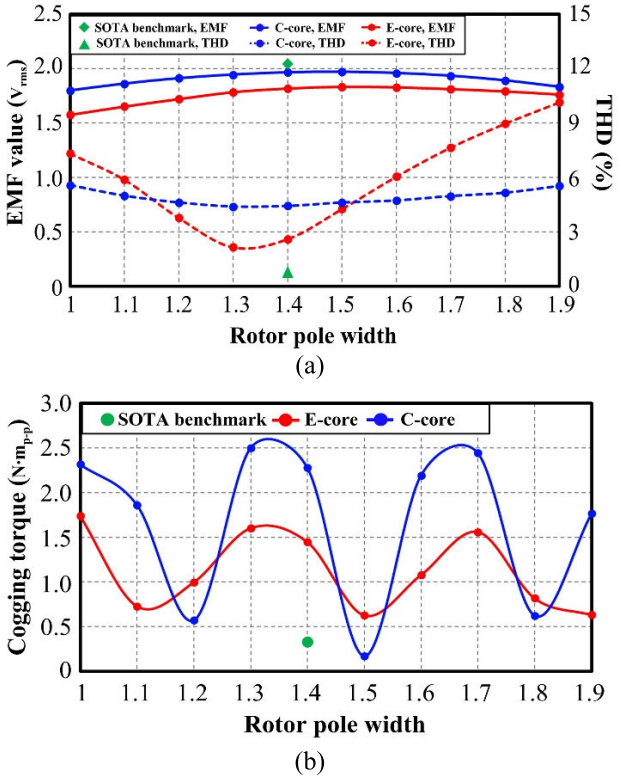


**FIGURE 7.** Influence of the rotor pole width on the no-load characteristics of SFPM generators. (a) Phase EMF (rms value, 1 turn) and THD. (b) Cogging torque.

### D. ROTOR POLE WIDTH RATIO

The rotor pole width has a significant impact the characteristics of the machine. Here, the ratio of the conventional

### E. NUMBER OF TURNS PER COIL

Given the design specifications for the E-core and C-core SFPM generators at a rated power of 2 kW and a phase

voltage of 96 V, it is necessary to adjust the number of turns per coil to attain this desired output. This adjustment is crucial as it directly affects the magnitude of the EMF, power factor, and the generator's ability to supply the load. In addition to the output power specification, the number of turns per coil is closely related to voltage regulation, which quantifies the generator's capacity to maintain a stable output voltage when faced with load variations. The on-load profiles of all proposed SFPM generators, evaluated at their optimal values for the number of rotor poles, split ratio, and rotor pole width, are depicted in Fig. 8. It demonstrates that both the output power and voltage regulation of the proposed generators increase as the number of turns per coil rises. However, the voltage regulation factor exhibits a more rapid incline compared to the output power due to the substantial increase in winding reactance and the resulting voltage drop across the reactance. Based on these observations, the most appropriate number of turns per coil for the E-core and the C-core designs are selected to be 120 and 105, respectively. These selections are made to maximize the simulated output power while ensuring that the measured output power remains consistently around 2 kW rating condition, making the generators suitable for low-speed wind power generation.

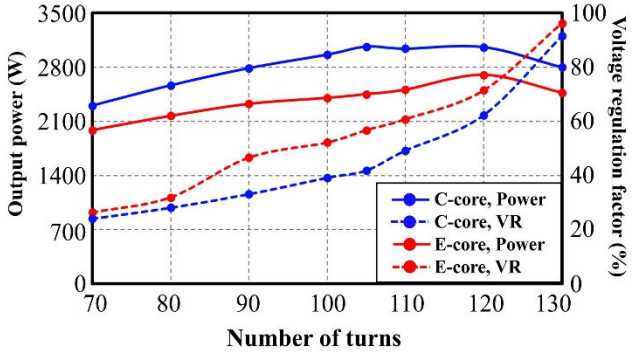


**FIGURE 8.** Influence of turn number per coil on output power and voltage regulation factor of the E-core and C-core SFPM generator.

## IV. GENERATOR PERFORMANCE ANALYSIS

In this section, the FEA-predicted output characteristics of the optimal designs, namely, the 12/23 E-core and 12/25 C-core SFPM structures, were analyzed and compared with those of the SOTA benchmark structure. The analysis covers both the no-load characteristics, such as flux line distribution, PM flux-linkage, phase EMF, as well as the on-load generating performance, including electromagnetic torque, torque ripple, losses, and efficiency. These investigations were conducted under rated conditions of 2 kW and 500 rpm.

### A. PM FLUX LINE DISTRIBUTION

Figs. 9(a)–9(c) show the $d$-axis no-load flux distribution of the SOTA benchmark structure, 12/23 E-core, and 12/25 C-core SFPM generators, respectively. An analysis reveals that the magnetic flux flowing through both stator and rotor teeth of the E-core and C-core generators has a higher concentration than the SOTA benchmark generator, primarily due to their shorter flux path. Also, the optimized C-core generator's shorter rotor height results in a reduced magnetic circulation path compared to other generators. Upon comparing the flux distribution at the stator core, the C-core generator exhibits a greater distributed magnetic flux compared to the E-core generator. The E-core generator, on the other hand, demonstrates a notably higher intensity of magnetic flux, leaving some space unutilized. As a result, these suggest that the C-core generator appears to achieve higher PM utilization in its design. Additionally, the E-core and C-core generators exhibit significantly lower leakage flux between adjacent stator and rotor teeth compared to the SOTA benchmark generator. This reduction in leakage flux can be attributed to the lower number of stator magnets and teeth in the E-core and C-core designs, resulting in a longer flux path and subsequently higher reluctance.

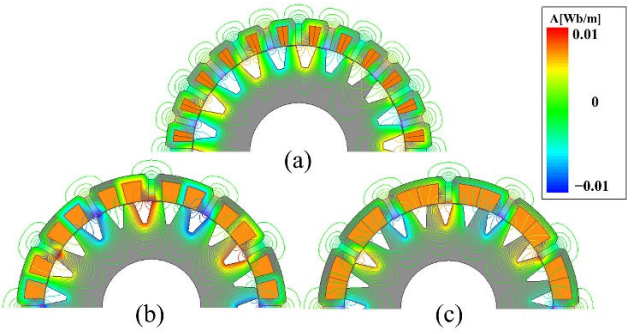


**FIGURE 9.** Open-circuit field flux distributions. (a) SOTA benchmark SFPM generator. (b) E-core SFPM generator. (c) C-core SFPM generator.

### B. PM FLUX-LINKAGE AND EMF

Fig. 10 illustrates a comparison of the PM flux-linkage between the optimal E-core and C-core structures and the SOTA benchmark structure. The analysis reveals that both the E-core and C-core SFPM generators exhibit a significantly higher PM flux-linkage compared to the SOTA benchmark, with increases of approximately 64.7% and 42.62% respectively. This higher PM flux-linkage is attributed to the increased magnetic flux density resulting from a higher number of installed winding turns per coil in the proposed designs.

The no-load phase EMF waveforms and their spectra of the three generators are shown in Fig. 11. It is evident that the proposed generators can generate substantially higher phase EMF compared to the SOTA benchmark generator. Also, the trend of the EMF waveforms is well consistent with that of the flux-linkage. From the result, proposed E-core and C-core SFPM generators can achieve peak phase EMF values of 311.12 V and 292.88 V respectively, which are 65.5% and 55.8% higher than the phase EMF of the SOTA benchmark generator. In addition, all three generators exhibit low 3rd harmonic components, resulting in greater symmetrical phase EMF characteristics.

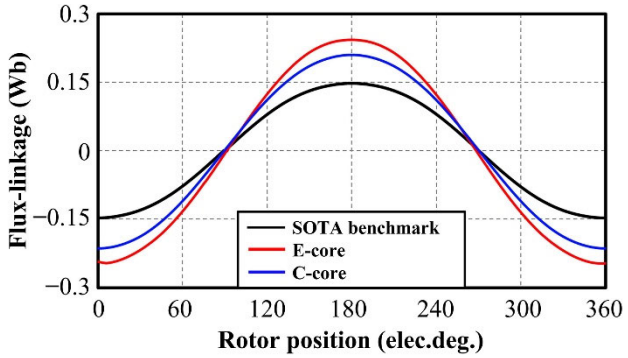


**FIGURE 10.** The no-load phase flux-linkage waveforms.

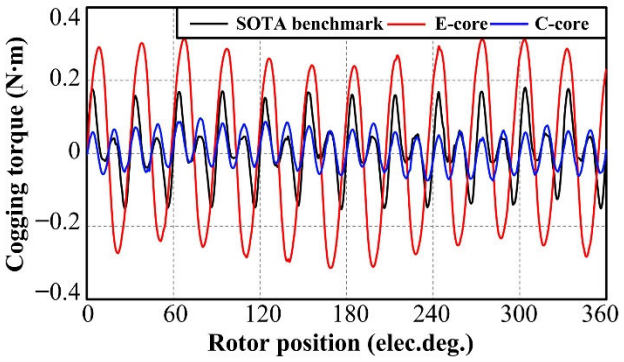


**FIGURE 12.** Cogging torque waveforms.

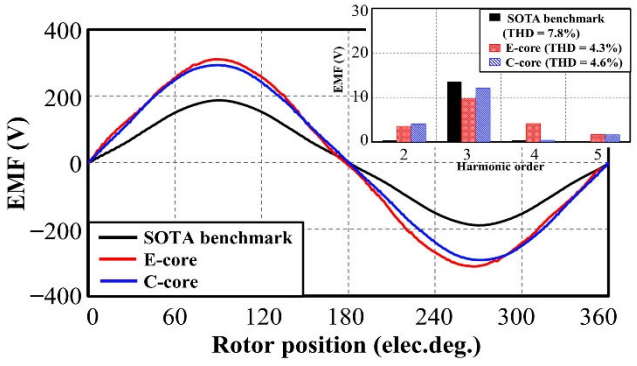


**FIGURE 11.** No-load phase EMF waveforms and its spectra.

### C. COGGING TORQUE

The cogging torque arises as a result of the interaction between the PMs and the salient rotor poles. It leads to mechanical vibrations during the starting and low-speed operation of the generator. The magnitude of the cogging torque can be calculated based on the energy stored in the air gap between the stator and rotor components. Fig. 12 depicts the cogging torque waveforms of the three SFPM generators. It is observed that the C-core generator exhibits a significantly lower cogging torque compared to both the SOTA benchmark and E-core generators. In particular, the cogging torque of the C-core generator is approximately half that of the SOTA benchmark structure. On the other hand, the high cogging torque of the E-core structure is primarily due to its E-shaped stator segment, which results in a higher density of magnetic flux on the salient poles. Therefore, the optimal C-core generator is more preferable than the other two machines during the starting conditions.

### D. ON-LOAD GENERATING PERFORMANCE

Fig. 13 illustrates the electromagnetic torque produced by the C-core SFPM generator, which reaches 63 N·m. this torque value surpasses the SOTA benchmark generator by 3.8%. On the other hand, the E-core SFPM generator demonstrates a slight decrease in torque, approximately 6.1% lower than the SOTA benchmark SFPM generator. Examining the torque waveforms of both the E-core and C-core SFPM generators, it becomes evident that they exhibit higher ripples compared to the SOTA benchmark generator. These ripples are primarily caused by unbalanced magnetic forces resulting from odd rotor poles. To provide a comprehensive overview, Table 2 summarizes the overall performance of all the generators under rating conditions achieved by FEA prediction. It shows that the 12-phase SOTA benchmark SFPM generator achieves the rated condition with a smaller current due to its higher number of phases. Unfortunately, the E-core generator exhibits a notably lower output power compared to its counterparts. Among the different generator types, the C-core generator exhibits the smallest copper loss, while the E-core generator experiences the largest copper loss due to its higher number of armature winding turns. Both the E-core and C-core generators have lower core losses compared to the SOTA benchmark structure, primarily due to a reduction in core material weight. However, the E-core and C-core generators experience higher PM eddy current losses compared to the SOTA benchmark generator due to the odd number of rotor poles causing an unevenly distributed air-gap magnetic permeance. Despite this, the C-core SFPM generator achieves the highest efficiency, reaching up to 93.6%. Remarkably, both the E-core and C-core generators demonstrate significant improvements in PM utilization, with an output power per PM volume enhancement of 74.6% and 98.4%, respectively, compared to the SOTA benchmark structure. Meanwhile, the EMF per unit turn per PM volume of the E-core and C-core generators surpasses that of the SOTA benchmark structure by 79.5% and 94%. This enhanced PM utilization of the E-core and C-core generators contributes to lower manufacturing costs. In terms of overload capability, both the E-core and C-core generators exhibit a higher voltage regulation factor. Figure 14 illustrates the analysis of the overload capability of the three SFPM generators. The slope of the SOTA benchmark generator is found to be less steep than that of the C-core and E-core generators, indicating its greater overload capability than others. The C-core generator, in particular, outperforms others in terms of EMF value and power generation at low load range. The high voltage regulation factor of the E-core and C-core generators can be attributed to their larger winding resistance and synchronous reactance, which increase with a greater number of coil

turns. Consequently, a future recommendation to address this weakness involves optimizing the structural parameters of the structure with paralleled coil configuration. Considering all factors, the trade-off analysis unequivocally demonstrates that the optimized 6-phase 12/25 C-core SFPM generator surpasses other designs in terms of performance and cost-effectiveness, making it a great choice for low-speed wind power generation. This generator design has been selected for prototyping.

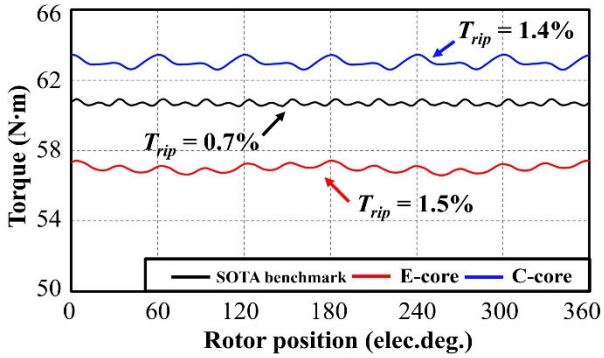


**FIGURE 13.** On-load electromagnetic torque waveforms at rated generating condition (500 rpm).

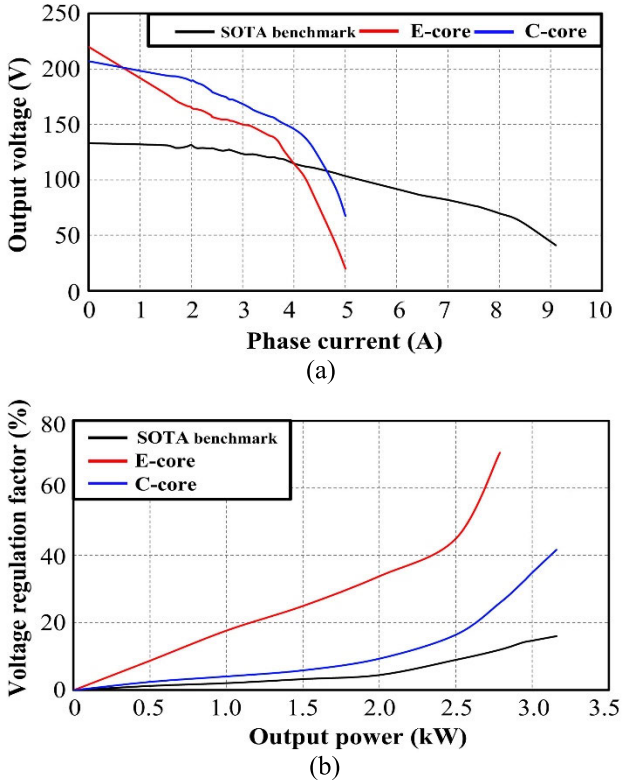


**FIGURE 14.** (a) Output voltage versus on-load phase current. (b) Voltage regulation factor versus output power (500 rpm).

### E. COMPARISON OF POWER GENERATING CAPABILITY TO THE PREVIOUS STUDIES

Given the objective of this study, which is to propose a high PM utilization PM generator, it is important to compare this indicator with existing PM generators in the literature. The power generation capability of the optimized 6-phase 12/25 C-core SFPM generator is compared with other radial-flux PM generators described in previous studies, as presented in Table 3. The comparison reveals that the proposed C-core SFPM generator achieves a power per PM volume of up to 24,979 kW/m$^3$, ranking it as the second-highest among all currently available PM generators. Furthermore, the power density of our proposed generators falls within an intermediate range. Consequently, it is evident that the optimized 6-phase 12/25 C-core SFPM generator represents a structure that has a very high PM utilization.

**TABLE 2.** Performance comparison at rating condition @500 rpm.

| Parameters | SOTA benchmark | E-core | C-core |
|---|---|---|---|
| Open-circuit phase EMF (rms,V) | 132.9 | 220.0 | 207.1 |
| EMF per unit turn per PM volume ($mV_{rms}/cm^3$) | 8.3 | 14.9 | 16.1 |
| Output voltage (rms,V) | 113.5 | 128.4 | 145.9 |
| Output current (rms,A) | 2.26 | 3.5 | 3.5 |
| Voltage regulation factor (%) | 17.1 | 71.4 | 41.9 |
| Output Power (W) | 3090.2 | 2699.8 | 3063.9 |
| Peak-peak cogging torque (N·m) | 0.33 | 0.63 | 0.17 |
| Average torque (N·m) | 60.7 | 57.0 | 63.0 |
| Torque ripple factor (%) | 0.7 | 1.5 | 1.4 |
| Copper loss (W) | 153.0 | 178.2 | 112.9 |
| Core loss (W) | 78.1 | 63.9 | 65.6 |
| PM eddy-current loss (W) | 22.0 | 25.9 | 22.7 |
| Power factor | 0.85 | 0.58 | 0.70 |
| Power per PM volume (W/cm$^3$) | 12.6 | 22.0 | 25.0 |
| Efficiency (%) | 92.1 | 90.4 | 93.6 |

**TABLE 3.** A comparison of power generating capability with other radial-flux PM generators.

| Reference | Power density (kW/m$^3$) | Power per PM volume (kW/m$^3$) |
|---|---|---|
| Proposed structure | 718.1 | 24,979 |
| [35] | 1,203.6 | 21,494 |
| [30] | 1,162.5 | 16,916 |
| [33] | 1,004.1 | 17,430 |
| [34] | 939.7 | 16,313 |
| [29] | 768.2 | 6,400.4 |
| [39] | 692.6 | 24,132 |
| [40] | 681.7 | 7,807 |
| [41] | 636.2 | 23,802 |
| [42] | 606.1 | 10,240 |
| [43] | 499.4 | 16,542 |
| [44] | 432.9 | 14,815 |
| [45] | 417.2 | 40,704 |
| [46] | 217.9 | 440.2 |

## V. EXPERIMENTAL VALIDATION

To validate the design and optimization, a prototype of the optimized 6-phase 12/25 C-core SFPM generator was manufactured and tested. The rotor and stator laminations, rotor, and stator of the generator prototype are shown in Fig. 15. To simplify manufacturing, an outer rib measuring 1 mm was incorporated at the outer diameter. This rib serves as a

connecting bridge between the C-shaped stator laminations and can be easily removed through grinding after assembly.

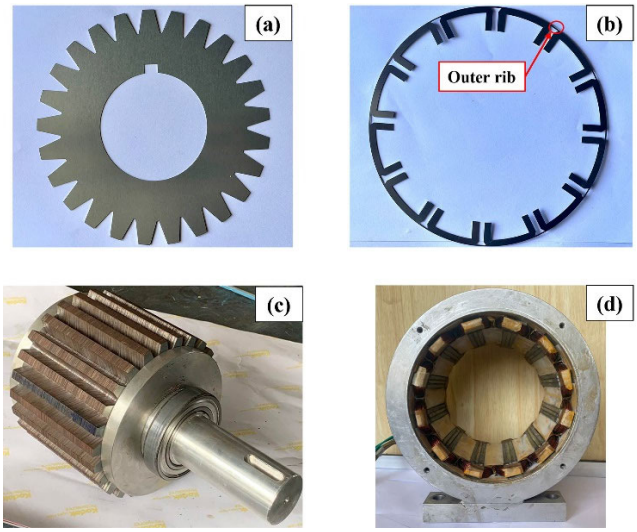


**FIGURE 15.** The 6-phase 12/25 C-core SFPM generator prototype. (a) Rotor lamination. (b) Stator lamination. (c) Rotor. (d) Stator.

### A. OPEN-CIRCUIT TEST

The open-circuit performance of the generator prototype was evaluated at a speed of 500 rpm. The measured three-phase open-circuit phase EMF produced by the winding set 1 of the 6-phase 12/25 C-core SFPM generator is illustrated in Fig. 16, while the EMF waveforms of phase A for the two sets are displayed in Fig. 17. The results demonstrate that the phase EMF waveforms are symmetrical and exhibit an electric frequency of 208.3 Hz. The magnitude of the EMF produced by the generator prototype measures 253.61 V. Fig. 18 compares the EMF waveform obtained from measurement and FEA prediction. Considering the influence of the outer rib, the measured open-circuit performance aligns well with the 2D-FEA results.

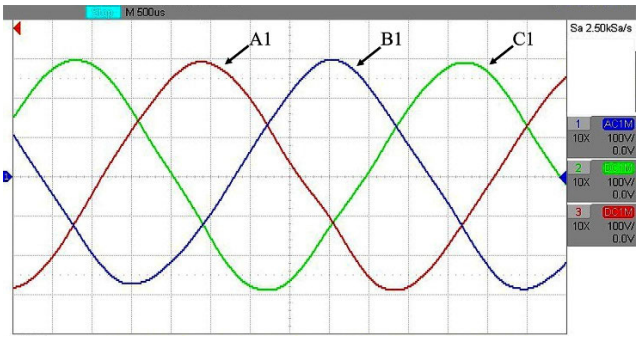


**FIGURE 16.** Measured three-phase open-circuit phase EMF waveforms produced by winding set 1 of the 6-phase 12/25 C-core SFPM generator at rated speed of 500 rpm.

### B. ON-LOAD TEST AT GENERATING MODE

Fig. 19 depicts the experimental setup of the 6-phase 12/25 C-core SFPM generator in generating mode. The prototype

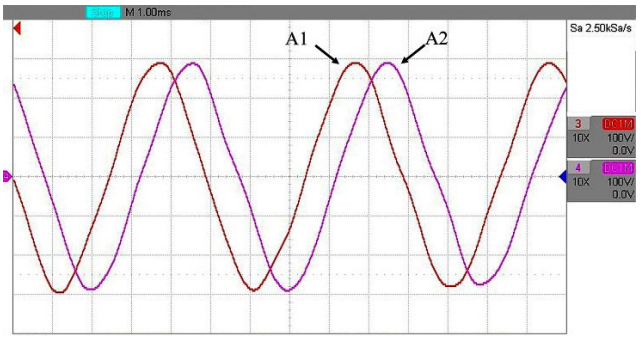


**FIGURE 17.** Measured open-circuit phase EMF waveforms produced by phase A of two winding sets of the 6-phase 12/25 C-core SFPM generator at rated speed of 500 rpm.

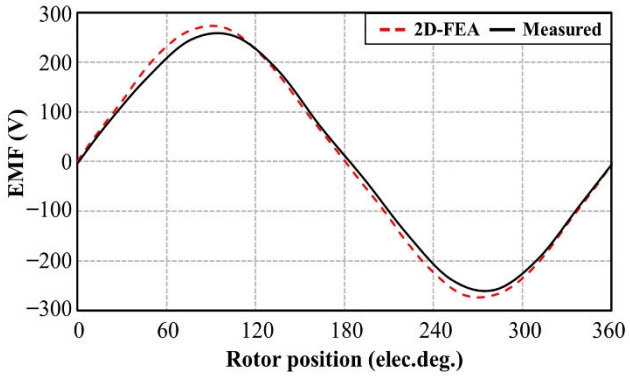


**FIGURE 18.** Measured and simulated open-circuit phase EMF of the 6-phase 12/25 C-core SFPM generator at 500 rpm.

**TABLE 4.** Comparison of performance indicators of the 6-Phase 12/25 C-Core SFPM generator at 500 rpm.

| Parameters | Unit | Measured | 2D-FEA (with outer rib) |
|---|---|---|---|
| Open-circuit phase EMF (rms) | V | 179.33 | 193.45 |
| Output voltage (rms) | V | 117.4 | 125.61 |
| Output current (rms) | A | 2.89 | 3.07 |
| Voltage regulation factor | % | 52.7 | 54 |
| Input Power | W | 2200 | 2464.44 |
| Output Power | W | 2035.72 | 2313.74 |
| Average torque | N·m | 41.51 | 45.53 |
| Torque ripple factor | % | 4.26 | 3.25 |
| Efficiency | % | 92.57 | 93.9 |

is connected to resistive loads of 40 Ω, with the resistance value calculated based on its rated specifications for facilitating the charging of a 96 V battery. The measured three-phase output voltage waveforms of winding set 1 at 500 rpm are presented in Fig. 20. These waveforms have an RMS value of 117.4 V, while the measured rated current is 2.89 A. The electromagnetic torque with the rated resistive load is measured by a torque sensor, the results are compared to the simulation result as shown in Fig. 21. The measured average electromagnetic torque is determined to be 41.51 N·m, whereas the analytical calculation predicts a

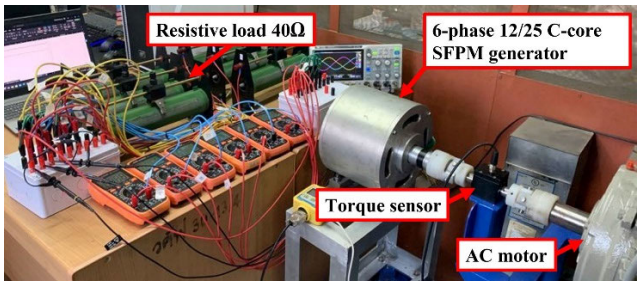


**FIGURE 19.** Test platform of the prototype working as generating mode.

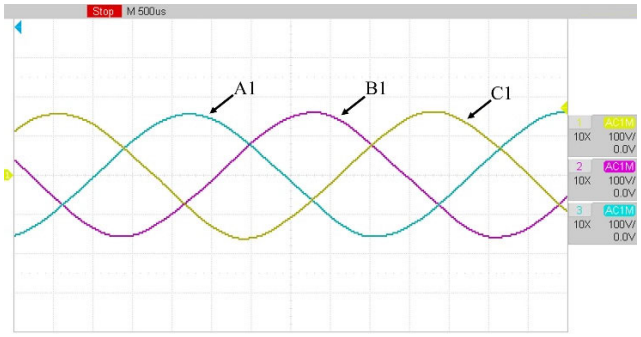


**FIGURE 20.** Measured phase voltage waveforms of prototype connected with rated resistive load at 500 rpm.

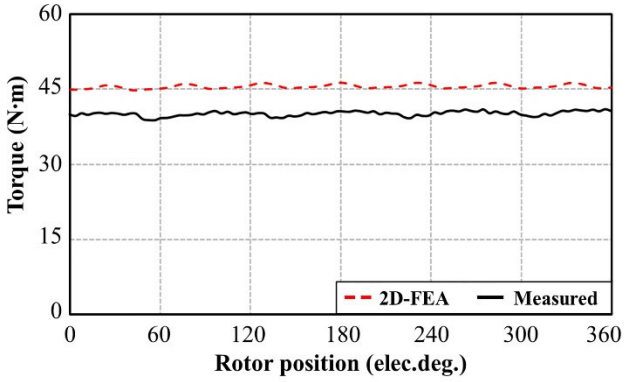


**FIGURE 21.** Comparison of measured and simulated torque waveforms of prototype connected with rated resistive load at 500 rpm.

value of 45.53 N·m. The disparity between the measurement and simulation can be attributed primarily to the effects of the end windings, manufacturing tolerances, and the neglect of axial leakage flux effects in the 2D-FEA. Table 4 presents the key performance indicators of the generator prototype obtained from measurements and simulations considering the effect of outer rib. It reveals that the 6-phase 12/25 C-core SFPM generator prototype is capable of producing rated output power of 2 kW when appropriately connected to a resistive load. The torque ripple and efficiency align closely with the FEA analysis. Overall, the measurement results, excluding tolerances, exhibit good agreement with the analytical calculations, thereby satisfying the design requirements.

## VI. CONCLUSION

A high PM utilization SFPM generator was designed for wind power generation, aiming for a rated output of 2 kW. The design involved the implementation of E-core and C-core techniques to enhance a SOTA benchmark 12-phase redundant SFPM generator. Key structural design parameters for two new 6-phase E-core and C-core SFPM generators were optimized. Under no-load conditions, the optimized 6-phase 12/25 C-core generator exhibited a significantly improved EMF with half the cogging torque compared to the SOTA benchmark generator. On the other hand, the E-core generator displayed a higher EMF but with larger cogging torque. Notably, the C-core SFPM generator exhibited the highest EMF per unit turn per PM volume and output power per PM volume, which was approximately twice that of the SOTA benchmark machine. The power per PM volume of generator ranked as the second-highest among all currently available PM generators. This high PM utilization was primarily achieved through an effective flux focusing effect. Meanwhile, the 6-phase 12/23 E-core SFPM generator demonstrated significantly improved PM utilization compared to the SOTA benchmark structure. Furthermore, the C-core SFPM generator achieved an impressive efficiency of up to 93.6%. The validation of the optimized 12/25 C-core prototype confirms the success of the design and optimization strategies presented in this research. These findings highlight the proposed C-core generator as a cost-effective solution with high PM utilization, making it suitable for low-speed wind power generation applications.

## REFERENCES

[1] C. N. Bhende, S. Mishra, and S. G. Malla, "Permanent magnet synchronous generator-based standalone wind energy supply system," *IEEE Trans. Sustain. Energy*, vol. 2, no. 4, pp. 361–373, Oct. 2011.

[2] M. Cheng, W. Hua, J. Zhang, and W. Zhao, "Overview of stator-permanent magnet brushless machines," *IEEE Trans. Ind. Electron.*, vol. 58, no. 11, pp. 5087–5101, Nov. 2011.

[3] V. Lounthavong, W. Sriwannarat, A. Siritaratiwat, and P. Khunkitti, "Optimal stator design of doubly salient permanent magnet generator for enhancing the electromagnetic performance," *Energies*, vol. 12, no. 16, p. 3201, Aug. 2019.

[4] C. Nissayan, P. Seangwong, S. Chamchuen, N. Fernando, A. Siritaratiwat, and P. Khunkitti, "Modeling and optimal configuration design of flux-barrier for torque improvement of rotor flux switching permanent magnet machine," *Energies*, vol. 15, no. 22, p. 8429, Nov. 2022.

[5] K. T. Chau, C. C. Chan, and C. Liu, "Overview of permanent-magnet brushless drives for electric and hybrid electric vehicles," *IEEE Trans. Ind. Electron.*, vol. 55, no. 6, pp. 2246–2257, Jun. 2008.

[6] W. Sriwannarat, A. Siritaratiwat, and P. Khunkitti, "Structural design of partitioned stator doubly salient permanent magnet generator for power output improvement," *Adv. Mater. Sci. Eng.*, vol. 2019, pp. 1–8, Apr. 2019.

[7] W. Zhao, L. Xu, and G. Liu, "Overview of permanent-magnet fault-tolerant machines: Topology and design," *CES Trans. Electr. Mach. Syst.*, vol. 2, no. 1, pp. 51–64, Mar. 2018.

[8] W. Sriwannarat, P. Seangwong, V. Lounthavong, S. Khunkitti, A. Siritaratiwat, and P. Khunkitti, "An improvement of output power in doubly salient permanent magnet generator using pole configuration adjustment," *Energies*, vol. 13, no. 17, p. 4588, Sep. 2020.

[9] A. S. Thomas, Z. Q. Zhu, and G. W. Jewell, "Comparison of flux switching and surface mounted permanent magnet generators for aerospace applications," in *Proc. 5th IET Int. Conf. Power Electron., Machines Drives*, Jul. 2010, pp. 111–116.
[10] A. Fasolo, L. Alberti, and N. Bianchi, "Performance comparison between switching-flux and IPM machines with rare-earth and ferrite PMs," *IEEE Trans. Ind. Appl.*, vol. 50, no. 6, pp. 3708–3716, Nov. 2014.
[11] H. Chen, A. M. El-Refaie, and N. A. O. Demerdash, "Flux-switching permanent magnet machines: A review of opportunities and challenges—Part I: Fundamentals and topologies," *IEEE Trans. Energy Convers.*, vol. 35, no. 2, pp. 684–698, Jun. 2020.
[12] S. Ning, P. Seangwong, N. Fernando, J. Jongudomkarn, A. Siritaratiwat, and P. Khunkitti, "A novel double stator hybrid-excited flux reversal permanent magnet machine with Halbach arrays for electric vehicle traction applications," *IEEE Access*, vol. 11, pp. 113255–113263, 2023.
[13] J. T. Chen, Z. Q. Zhu, S. Iwasaki, and R. Deodhar, "A novel E-core flux switching PM brushless AC machine," in *Proc. IEEE Energy Convers. Congr. Expo.*, Atlanta, GA, USA, 2010, pp. 3811–3818.
[14] J. T. Chen, Z. Q. Zhu, S. Iwasaki, and R. P. Deodhar, "Influence of slot opening on optimal stator and rotor pole combination and electromagnetic performance of switched-flux PM brushless AC machines," *IEEE Trans. Ind. Appl.*, vol. 47, no. 4, pp. 1681–1691, Jul. 2011.
[15] F. Yu, M. Cheng, and K. T. Chau, "Controllability and performance of a nine-phase FSPM motor under severe five open-phase fault conditions," *IEEE Trans. Energy Convers.*, vol. 31, no. 1, pp. 323–332, Mar. 2016.
[16] X. Xue, W. Zhao, J. Zhu, G. Liu, X. Zhu, and M. Cheng, "Design of five-phase modular flux-switching permanent-magnet machines for high reliability applications," *IEEE Trans. Magn.*, vol. 49, no. 7, pp. 3941–3944, Jul. 2013.
[17] A. S. Thomas, Z. Q. Zhu, R. L. Owen, G. W. Jewell, and D. Howe, "Multi-phase flux-switching permanent-magnet brushless machine for aerospace application," *IEEE Trans. Ind. Appl.*, vol. 45, no. 6, pp. 1971–1981, Nov. 2009.
[18] M. Taha, J. Wale, and D. Greenwood, "Design of a high power-low voltage multiphase permanent magnet flux switching machine for automotive applications," in *Proc. IEEE Int. Electr. Machines Drives Conf.*, May 2017, pp. 1–8.
[19] Y. Li, D. Bobba, and B. Sarlioglu, "Design and performance characterization of a novel low-pole dual-stator flux-switching permanent magnet machine for traction application," *IEEE Trans. Ind. Appl.*, vol. 52, no. 5, pp. 4304–4314, Sep. 2016.
[20] Y. Gao, D. Li, R. Qu, and H. Ding, "A double-stator flux switching PM machine with multi-PM MMF harmonics," *IEEE Trans. Magn.*, vol. 55, no. 6, pp. 1–6, Jun. 2019.
[21] G. Zhang, W. Hua, M. Cheng, and J. Liao, "Design and comparison of two six-phase hybrid-excited flux-switching machines for EV/HEV applications," *IEEE Trans. Ind. Electron.*, vol. 63, no. 1, pp. 481–493, Jan. 2016.
[22] W. Ullah and F. Khan, "Design and performance analysis of a novel outer-rotor consequent pole permanent magnet machine with H-type modular stator," *IEEE Access*, vol. 9, pp. 125331–125341, 2021.
[23] W. Yu, K. Liu, W. Hua, M. Hu, Z. Zhang, and J. Hu, "A new high-speed dual-stator flux switching permanent magnet machine with distributed winding," *IEEE Trans. Magn.*, vol. 58, no. 2, pp. 1–6, Feb. 2022.
[24] C. Chen, X. Ren, D. Li, R. Qu, K. Liu, and T. Zou, "Torque performance enhancement of flux-switching permanent magnet machines with dual sets of magnet arrangements," *IEEE Trans. Transport. Electrific.*, vol. 7, no. 4, pp. 2623–2634, Dec. 2021.
[25] P. Wang, W. Hua, G. Zhang, B. Wang, and M. Cheng, "Torque ripple suppression of flux-switching permanent magnet machine based on general air-gap field modulation theory," *IEEE Trans. Ind. Electron.*, vol. 69, no. 12, pp. 12379–12389, Dec. 2022.
[26] Z. Xiang, J. Ren, X. Zhu, X. Zhou, and L. Quan, "Broadening design and optimization of high-efficiency region for a dual-mechanical-port flux-switching permanent magnet motor," *IEEE Trans. Magn.*, vol. 58, no. 8, pp. 1–7, Aug. 2022.
[27] A. Abdelkefi, A. Souissi, I. Abdennadher, and A. Masmoudi, "On the analysis and torque enhancement of flux-switching permanent magnet machines in electric power steering systems," *World Electric Vehicle J.*, vol. 13, no. 4, p. 64, Apr. 2022.
[28] S. Eduku, Q. Chen, G. Xu, G. Liu, J. Liao, and X. Zhang, "A new fault-tolerant rotor permanent magnet flux-switching motor," *IEEE Trans. Transport. Electrific.*, vol. 8, no. 3, pp. 3606–3617, Sep. 2022.
[29] F. Li, W. Hua, M. Tong, G. Zhao, and M. Cheng, "Nine-phase flux-switching permanent magnet brushless machine for low-speed and high-torque applications," *IEEE Trans. Magn.*, vol. 51, no. 3, pp. 1–4, Mar. 2015.
[30] F. Li and X. Zhu, "Comparative study of stepwise optimization and global optimization on a nine-phase flux-switching PM generator," *Energies*, vol. 14, no. 16, p. 4754, Aug. 2021.
[31] B. A. Udochukwu and M. J. Kamper, "Evaluation of flux switching PM machines for medium-speed wind generator drives," in *Proc. IEEE Energy Convers. Congr. Expo.*, Sep. 2015, pp. 1925–1931.
[32] J. Ojeda, M. G. Simoes, G. Li, and M. Gabsi, "Design of a flux-switching electrical generator for wind turbine systems," *IEEE Trans. Ind. Appl.*, vol. 48, no. 6, pp. 1808–1816, Nov. 2012.
[33] L. Shao, W. Hua, Z. Q. Zhu, M. Tong, G. Zhao, F. Yin, Z. Wu, and M. Cheng, "Influence of rotor-pole number on electromagnetic performance in 12-phase redundant switched flux permanent magnet machines for wind power generation," *IEEE Trans. Ind. Appl.*, vol. 53, no. 4, pp. 3305–3316, Jul. 2017.
[34] L. Shao, W. Hua, F. Li, J. Soulard, Z. Q. Zhu, Z. Wu, and M. Cheng, "A comparative study on nine- and twelve-phase flux-switching permanent-magnet wind power generators," *IEEE Trans. Ind. Appl.*, vol. 55, no. 4, pp. 3607–3616, Jul. 2019.
[35] L. Shao, W. Hua, J. Soulard, Z.-Q. Zhu, Z. Wu, and M. Cheng, "Electromagnetic performance comparison between 12-phase switched flux and surface-mounted PM machines for direct-drive wind power generation," *IEEE Trans. Ind. Appl.*, vol. 56, no. 2, pp. 1408–1422, Mar. 2020.
[36] P. Seangwong, S. Chamchuen, N. Fernando, A. Siritaratiwat, and P. Khunkitti, "A novel six-phase V-shaped flux-switching permanent magnet generator for wind power generation," *Energies*, vol. 15, no. 24, p. 9608, Dec. 2022.
[37] Z. Q. Zhu and J. T. Chen, "Advanced flux-switching permanent magnet brushless machines," *IEEE Trans. Magn.*, vol. 46, no. 6, pp. 1447–1453, Jun. 2010.
[38] Y. Shi, L. Jian, J. Wei, Z. Shao, W. Li, and C. C. Chan, "A new perspective on the operating principle of flux-switching permanent-magnet machines," *IEEE Trans. Ind. Electron.*, vol. 63, no. 3, pp. 1425–1437, Mar. 2016.
[39] P. M. Tlali, R.-J. Wang, S. Gerber, C. D. Botha, and M. J. Kamper, "Design and performance comparison of Vernier and conventional PM synchronous wind generators," *IEEE Trans. Ind. Appl.*, vol. 56, no. 3, pp. 2570–2579, May 2020.
[40] B. Kim, "Design method of a direct-drive permanent magnet Vernier generator for a wind turbine system," *IEEE Trans. Ind. Appl.*, vol. 55, no. 5, pp. 4665–4675, Sep. 2019.
[41] C. J. J. Labuschagne and M. J. Kamper, "Design and performance evaluation of PM Vernier generator technology for a small-scale uncontrolled passive wind generator system," *IEEE Trans. Ind. Appl.*, vol. 58, no. 4, pp. 4657–4667, Jul. 2022.
[42] W. Ullah, F. Khan, and S. Hussain, "A novel dual rotor permanent magnet flux switching generator for counter rotating wind turbine applications," *IEEE Access*, vol. 10, pp. 16456–16467, 2022.
[43] X. Zhao, S. Niu, and W. Fu, "Sensitivity analysis and design optimization of a new hybrid-excited dual-pm generator with relieving-DC-saturation structure for stand-alone wind power generation," *IEEE Trans. Magn.*, vol. 56, no. 1, pp. 1–5, Jan. 2020.
[44] R. Nasiri-Zarandi, A. M. Ajamloo, and K. Abbaszadeh, "Design optimization of a transverse flux Halbach-array PM generator for direct drive wind turbines," *IEEE Trans. Energy Convers.*, vol. 35, no. 3, pp. 1485–1493, Sep. 2020.
[45] H. Geng, X. Zhang, L. Tong, Q. Ma, M. Xu, Y. Zhang, and L. Wang, "Performance optimization analysis of hybrid excitation generator with the electromagnetic rotor and embedded permanent magnet rotor for vehicle," *IEEE Access*, vol. 9, pp. 163640–163653, 2021.
[46] P. Seangwong, A. Siritaratiwat, W. Sriwannarat, N. Fernando, and P. Khunkitti, "Design of doubly salient permanent magnet generator for output power enhancement using structural modification," *J. Appl. Comput. Mech.*, vol. 7, pp. 2171–2178, Oct. 2021.

**PATTASAD SEANGWONG** received the B.S., M.S., and Ph.D. degrees in electrical engineering from Khon Kaen University, Khon Kaen, Thailand, in 2018, 2020, and 2023, respectively. His research interests include the diverse range of areas, including electrical machines, permanent magnet machines, electric vehicles, electrical motors, electrical generators, and renewable energy.

**NUWANTHA FERNANDO** (Member, IEEE) received the B.Sc. degree in electrical engineering from the University of Moratuwa, Sri Lanka, in 2008, and the Ph.D. degree from The University of Manchester, U.K., in 2012. He was a Researcher with the University of Nottingham and the University of Oxford. He is currently a Lecturer with RMIT University, Melbourne. His primary research interests include electric machines and drives, with a specific emphasis on applications in electric transportation. Additionally, he contributes as an Editor of IEEE TRANSACTIONS ON ENERGY CONVERSION.

**APIRAT SIRITARATIWAT** received the B.Eng. degree in electrical engineering from Khon Kaen University, Thailand, in 1992, and the Ph.D. degree from The University of Manchester, U.K., in 1999. Subsequently, he gained industry experience and worked for a few years. In 1994, he joined the Department of Electrical Engineering, Khon Kaen University. He is currently associated with the KKU-Seagate Cooperation Research Laboratory, Department of Electrical Engineering, Faculty of Engineering, Khon Kaen University. He has been an Active Researcher in the fields of electrostatic discharge/electrical overstress (ESD/EOS) and electromagnetic interference (EMI) and he has an impressive record of over 100 publications in these areas. Moreover, he is recognized as one of the pioneering researchers in the field of magnetism in Thailand. His significant contributions to this area include extensive work with Hard Disk Drive (HDD) industries.

**PIRAT KHUNKITTI** (Member, IEEE) received the B.Eng. (Hons.) and Ph.D. degrees in electrical engineering from Khon Kaen University, Thailand, in 2012 and 2016, respectively. Currently, he is an Associate Professor with the Department of Electrical Engineering, Faculty of Engineering, Khon Kaen University. His research interests include the wide array of areas, including electrical machines, permanent magnet machines, electric vehicles, electrical motors, electrical generators, and renewable energy. He has been a recipient of numerous scholarships from the Thailand Research Fund and the National Research Council of Thailand. Additionally, he serves as an Editor for the *Asia-Pacific Journal of Science and Technology* and holds the role of an Assistant Editor for *Engineering and Applied Science Research*.